DOI: 10.1002/ejic.200701159

$Ru_2M(dpa)_4Cl_2$ (M = Cu, Ni): Synthesis, Characterization, and Theoretical Analysis of Asymmetric Heterometal String Complexes of the Dipyridylamide Family

Gin-Chen Huang,[a] Marc Bénard,*[b] Marie-Madeleine Rohmer,[b] Long-An Li,[c] Mei-Jyun Chiu,[a] Chen-Yu Yeh,[c] Gene-Hsiang Lee,[a] and Shie-Ming Peng*[a,d]

Keywords: Molecular wires / Mixed-metal complexes / Metal-metal interactions / Magnetic properties / Electrochemistry / Density functional calculations

Four heterotrinuclear strings of metal atoms stabilized by dipyridylamide (dpa^-) ligands were synthesized and characterized. The metal frameworks of $Ru_2Cu(dpa)_4Cl_2$ (**1**), its monooxidized counterpart $[Ru_2Cu(dpa)_4Cl_2]PF_6$ (**2**), and their nickel homologues, $Ru_2Ni(dpa)_4Cl_2$ (**3**) and $[Ru_2Ni(dpa)_4Cl_2]PF_6$ (**4**), were shown by X-ray diffraction to be nonsymmetric, in spite of a severe disorder affecting the metal positions. The metal string is composed of a Ru dimer with a short Ru–Ru bond that is completed with the heterometal at a longer distance from the central ruthenium atom. This nonsymmetric structure was confirmed from NMR spectroscopy. The $[Ru_2M]^{6+}$ framework of **1** and **3** was shown from spectroelectrochemical analysis and DFT calculations to exist in the form of a mixed-valent $[Ru_2]^{5+}$ moiety coupled to a formally M^+ heterometal. The temperature-dependant magnetic susceptibility of these compounds is reported and interpreted by means of a model previously applied to $[Ru_2]^{5+}$ complexes. The redox chemistry of **1** and **3** was investigated by cyclic voltammetry, and the electronic structure of the mono- and dioxidized species was assigned from the observed changes in the UV/Vis spectra and from DFT calculations.

Introduction

Metal string complexes have recently attracted much attention due to their versatile structural and magnetic properties and to their potential applications in molecular electronics.[1–3] A large share of the recent studies on such complexes relies on the propensity of the polypyridylamido ligands with the general formula $[C_5H_4N\text{-}(N\text{-}C_5H_3N)_n\text{-}N\text{-}C_5H_4N]^{(n+1)-}$ to support a linear arrangement of the metal framework.[1] Recent advances in this field included the characterization of the first heterometallic frameworks supported by dipyridylamido (dpa^-) ligands, namely $CoPdCo(dpa)_4Cl_2$[4] and $CuMCu(dpa)_4Cl_2$ (M = Pd, Pt).[5] Such a juxtaposition of different metal atoms at bonding distance from each other is expected to produce unprecedented types of interactions, either covalent or magnetic. One of our goals is also to correlate these intermetallic interactions with the conductance measured at the molecular level[3] in order to design a real electronic device, such as a rectifier, within a single molecule (Scheme 1). We therefore report in this article the synthesis of four heterometallic strings held together by dpa^- ligands, namely $Ru_2Cu(dpa)_4Cl_2$ (**1**), $Ru_2Ni(dpa)_4Cl_2$ (**3**), and their oxidized counterparts $[Ru_2M(dpa)_4Cl_2]PF_6$ with M = Cu (**2**) and Ni (**4**). As for $Cr_2\cdots Fe(dpa)_4Cl_2$, which was quite recently reported by Nippe and Berry,[6] the metal framework in the present complexes is clearly nonsymmetric, with Cu in **1** and **2** or Ni in **3** and **4** lying at one end of the metal string. This asymmetry yielded severe disorder in the crystal structure, which prevented accurate structural characterization from X-ray diffraction. However, the nonsymmetric framework arrangement is confirmed by NMR, near-IR and EPR

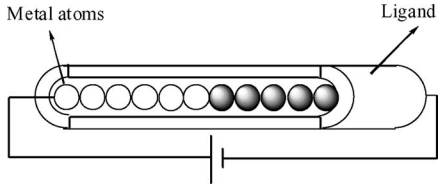

Scheme 1.

[a] Department of Chemistry, National Taiwan University, 1, Roosevelt Rd., Sec. 4, Taipei, Taiwan 106
Fax: +886-2-83693765
E-mail: smpeng@ntu.edu.tw
[b] Laboratoire de Chimie Quantique, Institut de Chimie, UMR 7177,
4, rue Blaise Pascal, 67000 Strasbourg, France
Fax: +33-390-241-30
E-mail: benard@quantix.u-strasbg.fr
[c] Department of Chemistry, National Chung Hsing University, Taichung, Taiwan
[d] Institute of Chemistry, Academia Sinica, Taipei, Taiwan 115, Taiwan

Supporting information for this article is available on the WWW under http://www.eurjic.org or from the author.

spectroscopic characterization. Magnetic measurements are reported and analysis of the electronic structure of the metal strings was carried out by DFT calculations.

Results and Discussion

Synthesis

Our strategy for preparing trinuclear string complexes in an asymmetric arrangement consisted in treating the dipyridylamine with a one-to-one mixture of a dimer exhibiting a metal–metal bond and a monomeric source of a different metal. It was expected that dpa^- would attach the monomer and the dimer together without breaking the metal–metal bond. The application of this protocol was straightforward in the case of **3**, which was obtained in moderate yield by heating $Ru_2(OAc)_4Cl$ with $Ni(OAc)_2{\cdot}4H_2O$ in the presence of dpa^- (Scheme 2). This procedure was repeated to obtain **1** by starting from either $Cu_2(OAc)_4{\cdot}2H_2O$ or $Cu(acac)_2$, but the yield was low and the product could not be crystallized. Complex **1** was eventually obtained, and crystallized, in a yield of 7–9%, starting from either CuCl or $CuCl_2$ in basic medium. The synthesis of **3**, and that of **1** when starting from $CuCl_2$, involves a global reduction, as previously observed in the formation of string complexes belonging to the same family.[7] The assignment of the transferred electron, either to the Ru dimer or to the heterometal, is discussed below.

Complexes **1** and **3** could be easily oxidized by adding ferrocenium hexafluorophosphate in dichloromethane (Scheme 2). Complex **1** and its oxidized counterpart **2** are very stable in air, as for $[Ru_2Ni(dpa)_4Cl_2]PF_6$ (**4**). However, **3** is not so stable and its UV spectrum changes when kept in solution for several days.

Crystal Structure and Computed Bond Lengths

The crystallographic data for **1**, **2**, **3**, and **4** are listed in Table 1 and an ORTEP view of **1** is displayed in Figure 1.

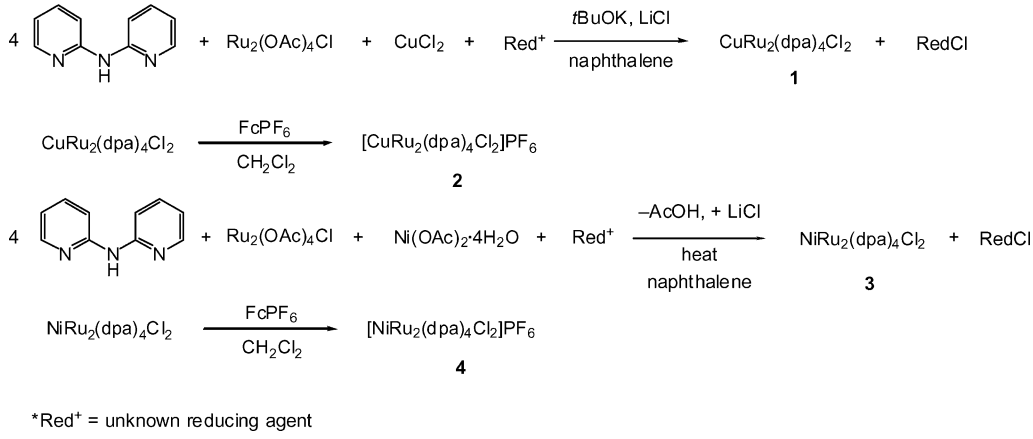

Scheme 2.

Table 1. Crystal structure of complexes **1**, **2**, **3**, and **4**.

	1·Et_2O	**2**·0.5MeOH·$2CH_2Cl_2$	**3**·Et_2O	**4**·0.5MeOH·$2CH_2Cl_2$
Formula	$C_{44}H_{42}Cl_2N_{12}CuORu_2$	$C_{42.5}H_{38}Cl_6CuF_6N_{12}O_{0.5}PRu_2$	$C_{44}H_{42}Cl_2N_{12}NiORu_2$	$C_{42.5}H_{38}Cl_6NiF_6N_{12}O_{0.5}PRu_2$
Mr	1091.48	1348.20	1086.65	1343.37
Crystal system	monoclinic	monoclinic	monoclinic	monoclinic
Space group	$P2_1/c$	$P2_1/n$	$P2_1/c$	$P2_1/n$
a [Å]	16.0858(2)	11.3937(2)	16.0020(2)	11.4175(1)
b [Å]	15.7749(2)	21.4425(4)	15.7598(2)	21.4424(3)
c [Å]	17.0286(2)	20.4295(4)	17.0071(2)	20.3587(3)
α [°]	90	90	90	90
β [°]	98.2366(7)	92.2979(11)	98.3586(8)	92.7752(8)
γ [°]	90	90	90	90
V [Å^3]	4276.47(9)	4987.10(16)	4243.43(9)	4978.34(11)
Z	4	4	4	4
T [K]	150(2)	150(2)	150(2)	150(2)
λ [Å]	0.71073	0.71073	0.71073	0.71073
$D_{calcd.}$ [g cm^{-3}]	1.695	1.796	1.701	1.792
R_1[a], wR_2[b] ($I>2\sigma I$)	0.0353, 0.0694	0.0721, 0.1654	0.0416, 0.1063	0.0535, 0.1334
R_1[a], wR_2[b] (all data)	0.0733, 0.0.826	0.1128, 0.1795	0.0753, 0.1203	0.0845, 0.1480

[a] $R_1 = \Sigma(||F_o| - |F_c||)/\Sigma|F_o|$. [b] $wR_2 = [\Sigma w(|F_o|^2 - |F_c|^2)^2/\Sigma w(F_o^2)]^{1/2}$.

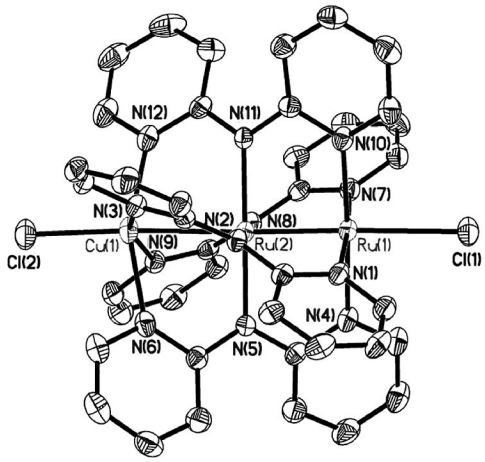

Figure 1. ORTEP view of the molecular structure of **1** (30% probability). Complex **3** is isostructural to **1**.

The asymmetric nature of both complexes induced a disorder in their metal framework. In the case of **1**, the Ru–Ru and Ru–Cu distances differ by ca. 0.2 Å, so that the positions of both metals at the end of the metal string can be distinguished, in spite of increased uncertainties. The disordered structures are equally distributed (Figure 2). Note, however, that the positions of the Cl and N atoms cannot be discriminated. Selected interatomic distances, both observed and computed, are displayed in Table 2. The Ru–Ru bond length is 2.246(3) Å, which is a very short distance in the range currently observed for multiply bonded $[Ru_2]^{4+}$ or $[Ru_2]^{5+}$ complexes (2.25–2.29 Å). Among the Ru dimers, the complex structurally closest to **1** is $Ru_2(PhNpy)_4Cl$ (Ru–Ru 2.275 Å), in which the phenylamidopyridyl ligand

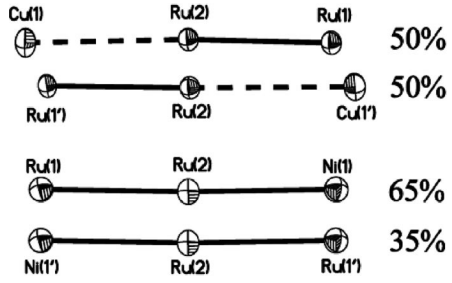

Figure 2. Relative occupancies of the disordered positions of the metal atoms in **1** (top) and **3** (bottom).

$(PhNpy)^-$ is derived from dpa^- by the replacement of a pyridine unit by a phenyl group.[8]

The Ru–N bond lengths in $Ru_2(PhNpy)_4Cl$ are 2.026 and 2.104 Å, and the longest distances are associated with the pentacoordinate ruthenium. They are in keeping with the distances of 2.046(2) and 2.136(4) Å observed in **1** for $Ru_{central}$–N and $Ru_{terminal}$–N, respectively. The Ru–Cl distance is rather long in **1**: 2.61–2.64 Å, relative to the value of 2.437 Å observed in the Ru dimer. Another closely related complex is $Ru_3(dpa)_4Cl_2$,[9] in which the Ru–Ru and Ru–Cl distances are 2.254 and 2.596 Å, respectively; the Ru–N bond lengths are 2.066 (central) and 2.108 Å (terminal). Note, however, that $Ru_3(dpa)_4Cl_2$ is diamagnetic,[9] at variance with **1** and **3**.

The Ru–Cu distance in **1** is 2.575(3) Å, which appears long in comparison with the current range of the metal–metal distances in $M_3(dpa)_4Cl_2$ complexes.[1] Conversely, the Cu–Cl bond is short [2.296(3) Å] with respect to the range of distances observed in $Cu_3(dpa)_4Cl_2$ (2.436–2.487 Å).[10] The most intriguing structural information however concerns the Cu–N bond length, which is assigned an average value of 2.173(3) Å and is much longer than the *outer* Cu–N distances observed in $Cu_3(dpa)_4Cl_2$ (2.06–2.09 Å).[10] In the latter complex, each terminal Cu^{II} atom displays the same square-pyramidal coordination as in **1**, and its $d_{x^2-y^2}$ orbital, antibonding with respect to N is occupied with one electron. This explains the elongation of the $Cu_{terminal}$–N bonds with respect to $Cu_{central}$–N (1.96–1.98 Å), in which this orbital remains unoccupied.[11] The extra elongation of Cu–N to 2.17 Å in **1** is therefore indicative of a *double* occupancy of the $d_{x^2-y^2}$ orbital of Cu and of the concomitant reduction of copper to Cu^I, as confirmed by the DFT calculations.

At variance with **1**, the positions of Ni and $Ru_{terminal}$ in **3** could not be distinguished, and they were arbitrarily fixed to the same position during the refinement process. Because of this constraint, the refined positions cannot be considered fully reliable, in spite of the low standard deviations (Table 2). The only reliable information is provided by the electron density, which is higher in the middle, showing that the central metal is ruthenium. The disordered structures are not equally distributed, and the metal occupancies are about 35 and 65% (Figure 2). The structure computed for the ground state of **3** shows a Ru–Ru distance that is still very short (2.337 Å) and a Ru–M distance that is appreci-

Table 2. Selected observed (average) and computed interatomic distances [Å] for $Ru_2Cu(dpa)_4Cl_2$ (**1**), $[Ru_2Cu(dpa)_4Cl_2]^+$ (**2**), $Ru_2Ni(dpa)_4Cl_2$ (**3**), and $[Ru_2Ni(dpa)_4Cl_2]^+$ (**4**).

	$\mathbf{1}_{obs.}$	$\mathbf{1}_{calcd.}$	$\mathbf{2}_{obs.}$	$\mathbf{2}_{calcd.}$	$\mathbf{3}_{obs.}$[a]	$\mathbf{3}_{calcd.}$	$\mathbf{4}_{obs.}$	$\mathbf{4}_{calcd.}$
Ru–Ru	2.246(3)	2.331	2.312(9)	2.308	2.341(4)	2.337	2.263(6)	2.317
Ru–M	2.575(3)	2.672	2.510(12)	2.641	2.349(5)	2.504	2.513(9)	2.587
Ru–Cl	2.624(3)	2.568	2.530(10)	2.492	2.513(9)	2.640	2.496(6)	2.460
M–Cl	2.296(3)	2.393	2.333(13)	2.422	2.462(10)	2.512	2.248(10)	2.329
Ru–N_{outer}	2.136(4)	2.138	2.092(12)	2.155	2.106(3)	2.145	2.109(9)	2.152
Ru–N_{inner}	2.046(2)	2.076	2.012(6)	2.053	2.012(3)	2.071	2.017(4)	2.054
M–N	2.173(6)	2.279	2.115(16)	2.141	2.102(3)	2.167	2.135(14)	2.173

[a] Constrained fitting: the $Ru_{terminal}$ and the Ni atom were fixed to the same position, which yields relatively small standard deviations. The real uncertainties of the structure should be much larger, especially along the Cl–Ni–Ru–Ru–Cl axis.

ably shorter with nickel (2.504 Å) than with Cu in **1**. This contraction of the Ru–M distance goes along with an elongation of the M–Cl distance (2.512 Å in **3**). A similar disorder affects the crystal structures of oxidized complexes **2** and **4**, which also results in poor accuracy. Density fits used correspond to 45/55% occupancy for each orientation of disorder. Although these structures are not reliable enough to be discussed in detail, they confirm the presence of monooxidized species with a hexafluorophosphate ion in the unit cell (Supporting Information, Figure S1).

In spite of the poor accuracy discussed above, the observed atomic positions are however accurate enough to provide a convenient starting point for DFT geometry optimization. DFT/B3LYP calculations previously carried out on the ground state of 1D complexes belonging to the same family reproduce the observed bond lengths with a slight systematic overestimation most often limited to a few picometers.[4,11–13] The discrepancies obtained in the present series of complexes tend to be larger and often reach 0.1 Å and even 0.155 Å for the Ru–Ni bond length in **3**. Given the problems encountered in the refinement of the atomic positions as a result of the disordered structures, we consider that the result of DFT geometry optimizations provides a more consistent collection of data to be used for a comparative analysis of structures. The atomic Cartesian coordinates optimized for the ground states of **1**, **2**, **3**, and **4** are therefore provided in the Supporting Information (Table S1) and computed values of the most important interatomic distances are displayed in Table 2. For **1**, the computed Ru–Ru bond length is 2.33 Å. The Ru–N bond lengths are 2.076 and 2.138 Å, and the longest distances are associated with the pentacoordinate ruthenium. The computed Ru–Cu distance (2.672 Å) indeed appears very long in comparison with the current range of the metal–metal distances in $M_3(dpa)_4Cl_2$ complexes, and the Cu–Cl distance (2.393 Å) remains shorter than average. Concerning the Cu–N bond length also discussed in detail above, the calculation confirms the double occupancy of the metal–ligand antibonding orbital and yields a distance of 2.279 Å, which is still larger than the average observed value by ca. 0.1 Å. Note, however, that the observed lengths of the four supposedly equivalent Cu–N bonds are scattered between 2.126 and 2.226 Å.

Bond lengths obtained from the DFT geometry optimization of **2** are not strikingly different from those of **1**, with one notable exception: the Cu–N distances contract upon oxidation from 2.279 to 2.141 Å (Table 2). At variance with this behavior, oxidation of the Ru_2Ni complex does not affect the metal–nitrogen bond lengths, but yields a significant increase in the Ru–Ni distance from 2.504 to 2.587 Å and a dramatic contraction of both metal–chlorine bonds from 2.640 to 2.460 Å for Ru–Cl and from 2.512 to 2.329 Å for Ni–Cl (Table 2).

NMR Spectrum

The ^{1}H NMR spectra of complexes **1** and **3** are reported in the Supporting Information (Figure S4). Both spectra display eight peaks. Symmetric metal string complexes coordinated by dpa^- ligands display spectra with only four lines. Conversely, the number of NMR signals is doubled to eight in trinuclear complexes that are clearly nonsymmetric, such as $Co_3(dpa)_4ClBr$.[14] The presence of eight different peaks in the spectrum of both neutral heterometallic complexes therefore provides further direct evidence of their asymmetric structure.

Computational Study

The sequence of metal orbitals in symmetric, trimetallic complexes of dipyridylamide has been introduced and discussed previously.[4,11,15] It is composed of five groups of three MOs corresponding to the bonding, nonbonding, and antibonding combinations of the atomic d orbitals. Two of these groups are composed of δ-type orbitals characterized by a weak intermetallic overlap. By assuming that the local axis systems attached to the metal atoms in the *x* and *y* directions are collinear with the metal–nitrogen bonds and that the *z* axis is collinear with the metal string, the group of low-energy *δ* MOs is composed of d_{xy}-like atomic orbitals with small, π-type interactions with the equatorial nitrogen ligands. Another group of three δ MOs involves the $d_{x^2-y^2}$-like metal orbitals, and it develops strong antibonding, σ-type interactions with the equatorial ligands. Because of these interactions, this group of MOs is usually highest in energy. In homometallic complexes of regular dipyridylamide ligands, the magnetic and structural properties are therefore monitored by the number of electrons originating from the $[M_3]^{6+}$ framework to be accommodated on these 15 MOs. Complexes with 18 metal electrons or less, such as $Cr_3(dpa)_4Cl_2$ and $Ru_3(dpa)_4Cl_2$, populate the bonding and some nonbonding levels, which thus gives rise to strong interactions with multiple, delocalized M–M–M bonding character.[9,16] With 21 d electrons, $Co_3(dpa)_4Cl_2$ is on the verge between two electronic states: one corresponding to a delocalized two-electron, three-center bonding interaction, which gives rise to a symmetric conformation, and the other leading to the separation of the metal framework into a closed-shell dimer exhibiting σ bonding and a weakly interacting, high-spin Co atom.[12] Finally, the $M_3(dpa)_4Cl_2$ and $[M_3(dpa)_4Cl_2]^+$ complexes with more than 21 metal electrons (M = Ni, Cu) give rise to antiferromagnetic interactions involving a partial occupancy of the high-lying, metal–nitrogen antibonding δ MOs and a superexchange mechanism through the dpa^- ligands.[10,11,13]

Introduction of a heterometallic framework is likely to modify this predictable drift from a delocalized bond to an antiferromagnetic interaction when increasing the number of d electrons. For instance, the presence of palladium at the center of the first such compound to be characterized, $CoPdCo(dpa)_4Cl_2$, strongly constrains both terminal Co atoms to adopt a high-spin electronic configuration rather than taking part in a delocalized four-electron, three-center σ bond.[4] Besides, the present complexes combine a dimer of Ru^{II}, which tends to give strong Ru–Ru bonds, with a

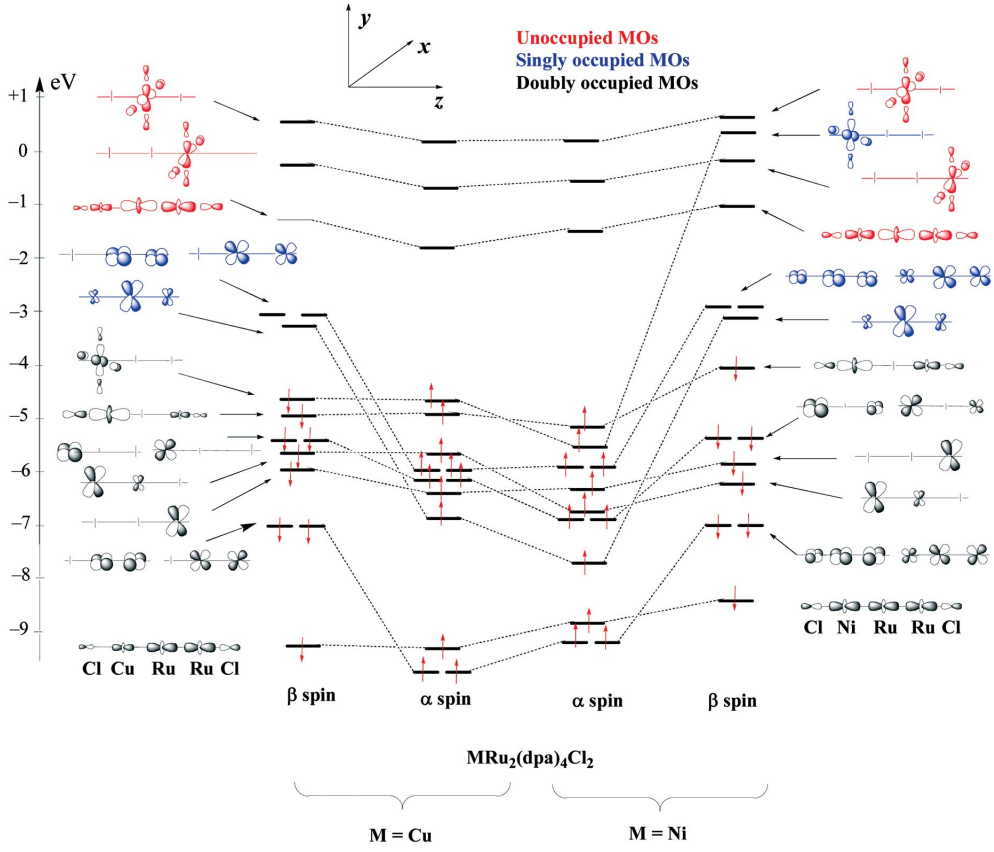

Figure 3. Diagram of the frontier orbitals with major metal character obtained from unrestricted DFT calculations for the quartet ground state of **1** (left-hand side) and for the quintet ground state of **3** (right-hand side). Energy scale is in eV.

late-transition metal in principle less prone to covalent bonding.

Figure 3 displays the sequence of metal energy levels obtained from unrestricted DFT/B3LYP calculations carried out on **1** and **3**. A similar diagram devoted to oxidized species **2** and **4** is available in the Supporting Information (Figure S5). The variation in the strength of the metal–metal and metal–ligand bonds in the four complexes is illustrated in Table 3 by the corresponding Mayer bond indices.[17]

Table 3. Selected Mayer bond orders computed for complexes **1**, **2**, **3**, and **4**.

	1	**2**	**3**	**4**
Ru–Ru	0.986	0.934	0.898	0.823
Ru–M	0.235	0.016	0.316	0.122
Ru–Cl	0.864	0.958	0.810	0.997
M–Cl	0.916	0.992	0.829	0.982
Ru_{term}–N	0.484	0.494	0.484	0.498
Ru_{mid}–N	0.576	0.562	0.564	0.564
M–N	0.342	0.595	0.458	0.540

The presence of a significant HOMO–LUMO gap, the consistency of the optimized geometries with the trends that could be extracted from the disordered crystal structures, and the agreement of the computed molecular spin states (S = 3/2 for **1**, S = 2 for **3**) with magnetic measurements gives good confidence that the MO diagram of Figure 3 describes the ground state of both neutral compounds. Analysis of the 15 MOs associated with the metal framework of **1** clearly shows that the trimetallic core splits into weakly interacting moieties: a $[Ru_2]^{5+}$ fragment with the electronic configuration $(\sigma)^2(\pi)^4(\delta)^2(\delta^*)^1(\pi^*)^2$, which is reminiscent of $Ru_2(\mu\text{-}O_2CR)_4Cl$ complexes, and a Cu atom that was formally reduced to Cu^I and which has d^{10} electronic configuration. The only trace of a metal–metal bond between copper and the Ru dimer appears as a mirror image in the LUMO, which corresponds to the σ* MO and is mainly concentrated on the $[Ru_2]^{5+}$ fragment, but displays some Cu–Ru antibonding character (Figure 3, left side). The presence of such a residual σ bond is confirmed by the non-negligible value of the Mayer bond order associated with Ru–Cu (0.235, Table 3). Note that the d^{10} electronic configuration of copper implies a double occupancy for the $d_{x^2-y^2}$-like orbital of copper. This Cu–N antibonding orbital is indeed the HOMO in both spinorbital subsets (Figure 3), and such a double occupancy, still unprecedented in the family of polypyridylamide complexes, explains the remarkably long Cu–N distances computed for **1** (2.279 Å, Table 2). Indeed, the oxidation process leading to complex **2** removes an electron from this orbital; this yields a quintet ground state for **2** with noticeably shorter Cu–N distances (Figure S5). These distances are in keeping with those corresponding to $Cu_3(dpa)_4Cl_2$.[10,11] The associated Mayer bond index consistently blows up in the process from a low 0.342 to 0.595 (Table 3). Note also the concomitant weak-

ening of the residual Cu–Ru bond, which is illustrated by the near-zero value of the bond index in **2** (Table 3).

Complex **3** formally displays an electronic structure similar to that of **1**, that is, a $[Ru_2]^{5+}$ fragment coupled with a nickel atom in oxidation state I. Indeed, the resulting ground state is a quintet, in which all MOs that should be formally assigned to nickel are doubly occupied, except for the $d_{x^2-y^2}$-like orbital, which is singly occupied. At variance with **1**, however, the formal oxidation of the Ru dimer as $[Ru_2]^{5+}$ is compensated in part by an extension to nickel of the Ru–Ru bonding interactions. The unoccupied σ* MO now incorporates a more important contribution from nickel, and so for the singly occupied π* MOs (Figure 3, right-hand side). Quite logically, the Ru–M distance is computed to be much shorter with M = Ni (2.504 Å) than with M = Cu (2.672 Å) (Table 2), and the corresponding bond index increases to 0.316 (Table 3). As for **1**, oxidation of **3** occurs on the heterometal: the electron is removed from the doubly occupied, nonbonding σ MO, which is mainly localized on nickel with an important contribution of the terminal Ru atom (Figure 3). The ground state of $[Ru_2Ni(dpa)_4Cl_2]^+$ (**4**) is therefore a sextet state that involves σ and π bonding interactions between the $[Ru_2]^{5+}$ and Ni^{II} moieties (Figure S5). As already pointed out in the comparison of the computed bond lengths, the structural consequences of oxidation are quite different for **2** and **4**. As oxidation of **1** occurs on the Cu–N antibonding MO, the reorganization of the metal framework and that of the coordination sphere remains limited, except for an important contraction (0.138 Å) of the Cu–N distances. Because the oxidation of **3** affects the nonbonding σ_{nb} MO, the Ru–N and Ni–N bond lengths are not affected, but the partial depopulation of σ_{nb}, which is antibonding with respect to chlorine, induces an important contraction of the Ru–Cl and Ni–Cl bond lengths (Table 2), still enhanced by the positive net charge on the metal framework. The significant increase in the M–Cl bond indices is in keeping with this analysis (Table 3).

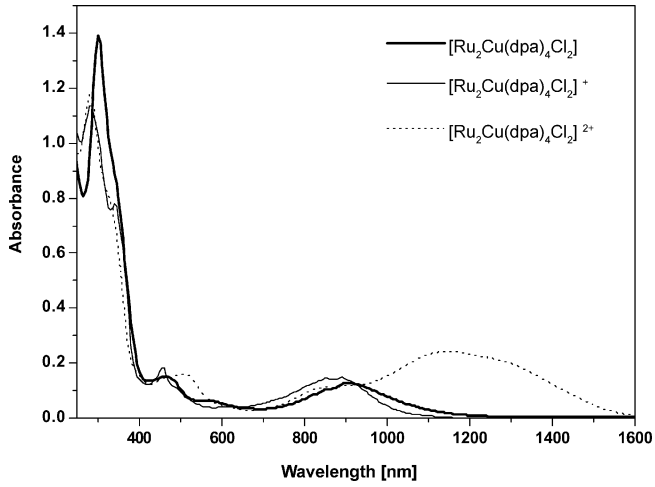

Figure 4. UV/Vis spectral changes associated with the electrochemically generated neutral, first, and second oxidations of 1 mM compound **1** in 0.1 M TBAP/CH_2Cl_2 at 25 °C. The applied potentials were –0.09 V for the neutral, 0.13 V for the monooxidized, and 1.24 V for the doubly oxidized species.

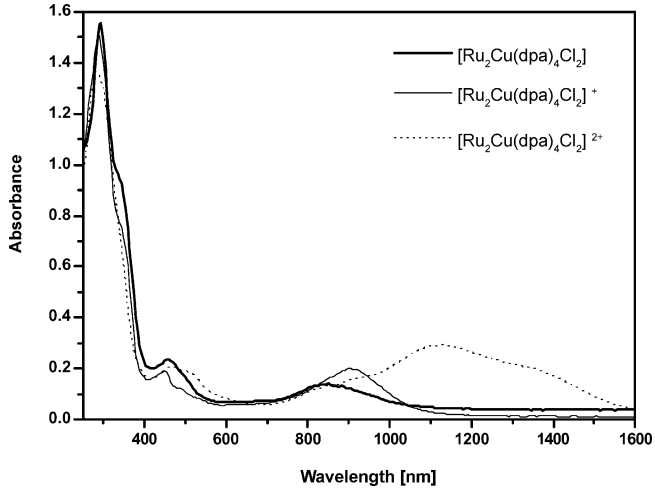

Figure 5. UV/Vis spectral changes associated with the electrochemically generated neutral, first, and second oxidations from 1 mM compound **3** in 0.1 M TBAP/CH_2Cl_2 at 25 °C. Applied potentials were 0.16 V for the neutral, 0.32 V for the monooxidized, and 1.20 V for the doubly oxidized species.

Near-IR and UV/Vis Spectra

The spectrum of complexes **1** and **3** at a concentration of 0.1 mM and its evolution associated with one-electron and two-electron oxidation processes were studied in the region 250–1700 nm by means of the OTTLE (optical transparent thin layer electrochemical) technique. The supporting electrolyte was TBAP (tetrabutylammonium perchlorate, 0.1 M) in CH_2Cl_2 at 25 °C, and appropriate potentials were applied for each species. OTTLE spectra for **1**, **3**, and their respective oxidized species are displayed in Figures 4 and 5. The UV spectrum of complexes **1**, **2**, **3**, and **4** were also obtained from standard techniques and proved similar to the OTTLE-generated spectrum.

The spectrum of **1** displays a peak in the near-IR region (≈900 nm), which seems typical of a mixed-valence behavior. The presence of such a peak is quite unusual in neutral complexes of standard polypyridylamide ligands, in which the formal M^{2+} configuration of all metal atoms has been steadily confirmed up to now from spectroscopic characterization as from molecular orbital analysis. The electronic configuration referred to as Type I (Scheme 3), in which all metals are divalent, was therefore expected for **1**, but the presence of the uncommon near-IR peak suggests the occurrence of a different electronic organization with a $[Ru_2]^{5+}$ unit and a monovalent copper (Type II, Scheme 3). The Ru–Ru fragment in the Type II electronic structure is then reminiscent of the diruthenium complexes $Ru_2(\mu\text{-}O_2CR)_4Cl$ that display a near-IR band close to 1000 nm,[18] and they were shown from spectroscopy and theoretical analysis[19] to have the electronic configuration $(\sigma)^2(\pi)^4(\delta)^2(\delta^*)^1(\pi^*)^2$. By contrast, the near-IR band vanishes in $Ru_2(\mu\text{-}O_2CR)_4$ complexes, which have a closed-shell elec-

tronic structure in which the δ* MO is fully occupied and the π* MO is empty.[20] The preference for the oxidation of the diruthenium unit into $[Ru_2]^{5+}$ with respect to a $Cu^{I} \rightarrow Cu^{II}$ process is quite conceivable in view of the well-documented semicore character of the 3d shell of copper.

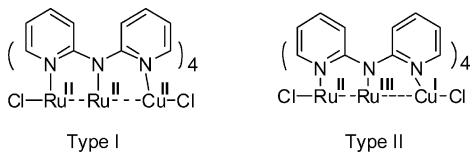

Scheme 3.

The near-IR band is still present in Ru_2Ni complex **3**, and it has a half width of 2797 cm^{-1} (Figure 5). Figures 4 and 5 show that this band does not disappear upon oxidation and even becomes slightly broader for oxidized complex **4**, in which this band has a half width of 2865 cm^{-1}. This band should therefore correspond to an internal transition in the diruthenium fragment, which implies a formal exchange of the oxidation states II and III assigned in Scheme 3 (Type II) to the terminal and to the central Ru atoms, respectively. DFT calculations corroborate the mixed-valent Type II electronic structure for complexes **1** and **3** as for their oxidized counterparts, as discussed in the computational section. The orbital diagram displayed in Figure 3 shows that the most probable assignment for such an intervalence band corresponds to a transition arising from the doubly occupied δ, d_{xy}-like MO localized on the *terminal* Ru atom, calculated at ca. –6.0 eV in **1**, toward the singly occupied δ MO localized on the *central* Ru atom. A similar orbital arrangement does exist for **3** as for the oxidized counterparts of **1** and **3**, as the first oxidation process involves an electron localized on the non-ruthenium metal. Such a transition has no equivalent in any *neutral* complex of dpa^- characterized previously. However, such a band is generated, with a maximum at 922 nm, from the oxidation process of $Ru_3(dpa)_4Cl_2$,[9] which suggests the formation of a mixed-valent Ru dimer.

Electrochemistry

As with many diruthenium and triruthenium complexes, compounds **1** and **3** display rich redox chemistry, as evidenced by the cyclic voltammogram of Figure 6. Measurements were carried out at 25 °C with 0.1 M TBAP/DCM as electrolyte.

Two reversible redox couples appear at $E_{1/2}$ = +1.07, +0.19 V, and one irreversible peak at –0.6 V for complex **1**, vs. Ag/AgCl. The halfwave potentials of the reversible events are shifted to $E_{1/2}$ = +1.06, +0.02 V in complex **3**. In many $[Ru_2]^{5+}$ complexes, one or two peak(s) corresponding to reversible events are generally observed between 0 and –1.1 V and assigned to reduction processes.[21] The occurrence and the assignment of the peaks is likely to be different in **1**, for which the highest-occupied molecular orbital has practically all of its weight on the copper atom and its equatorial coordination environment, according to the

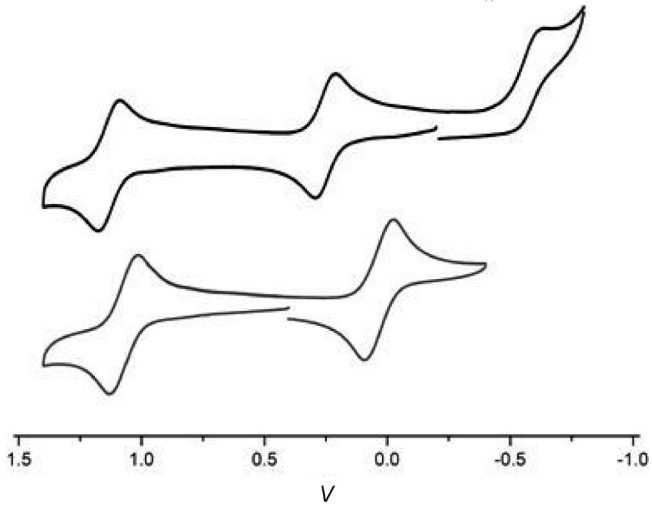

Figure 6. Cyclic voltammetry of complexes **1** (top) and **3** (bottom) in DCM and 0.1 M TBAP as supporting electrolyte.

DFT calculations. In accordance with the orbital diagram of Figure 3, we therefore assign the peak at 0.19 V to a Cu^{I}/Cu^{II} oxidation process. This is also in agreement with the analysis of Figure 4, which does not detect any change in the $[Ru_2]^{5+}$ intervalence transfer band upon the first oxidation process. The oxidation energies computed for **1** and **3** are 5.37 and 4.73 eV, respectively. Compound **3** is therefore easier to oxidize, which is in agreement with a corresponding lower halfwave potential.

Analysis of the spectral changes observed in the region of the second oxidation of **1** (1.04–1.20 V) shows the appearance in $[Ru_2Cu(dpa)_4Cl_2]^{2+}$ of a broad peak near 1100 nm (Figure 4). The growth of a similar peak is observed during the oxidation of $[Ru_3(dpa)_4Cl_2]^{+}$.[9] The raise of a transition in such a low-energy range could be associated to the lift of the orbital degeneracy caused by a first-order Jahn–Teller effect. The presence of a semioccupied π* MO centered on the Ru dimer in **2** suggests that the second oxidation event associated with the peak at +1.07 V might originate in this orbital. Although the MO analysis of $[Ru_3(dpa)_4Cl_2]^{+}$ has not been reported, a similar situation could be expected from the presence of a delocalized π* MO among the frontier orbitals of the neutral complex.[9] A peak appears in the same region of the IR spectrum during the oxidation of complex **4** and a similar assignment is proposed to involve the semioccupied π* MO, now somewhat delocalized over the nickel atom (Figure 3). However, the first peak of the voltammogram, observed in the vicinity of 0.0 V should originate in the σ nonbonding HOMO, which has its major weight on nickel (Figure 3).

Magnetic Measurements and EPR Spectra

Early investigation of the variable-temperature magnetic susceptibility of $Ru_2(\mu\text{-}O_2CnPr)_4Cl$ showed that the complex behaves according to the Curie–Weiss law over the 35–300 K temperature range, but significantly deviates from this behavior below 35 K. Different models were used to fit

the data and two of them were deemed to be reasonably good. Both neglected the intermolecular interactions possibly induced by the polymeric nature of these complexes, which suggests, for the deviations, an intramolecular origin induced by a large zero-field splitting (ZFS) within the $[Ru_2]^{5+}$ dimer (S = 3/2).

The first model considers the full-spin Hamiltonian for an S = 3/2 system [Equation (1)]:

$$H = \beta(g_x H_x S_x + g_y H_y S_y + g_z H_z S_z) + D[S_z^2 - (1/3)S(S+1)] + E(S_x^2 - S_y^2) \quad (1)$$

where D and E are scalar crystal-field splitting parameters. The matrix elements for this Hamiltonian were given by Telser and Drago.[22] The second model involves the exponential term the zero-field susceptibility of an S = 3/2 complex with O_h symmetry together with axial zero-field splitting, as originally derived by O'Connor:[23]

$$\chi_{\parallel} = \frac{Ng_{\parallel}^2\beta^2}{kT}\frac{1+9\exp(-2D/kT)}{4[1+\exp(-2D/kT)]}$$
$$\chi_{\perp} = \frac{Ng_{\perp}^2\beta^2}{kT}\frac{4+(3kT/D)[1-\exp(-2D/kT)]}{4[1+\exp(-2D/kT)]} \quad (2)$$

assuming an orientational average $\chi_{av} = (x_{\parallel} + 2x_{\perp})/3$ was used.

Both models were found to provide fittings of similar quality. The parameters obtained for $Ru_2(\mu\text{-}O_2CnPr)_4Cl$ with the second model [Equation (2)] are reproduced in Table 4. The same model was used to fit the temperature magnetic susceptibility of complex **1**. The observed susceptibility and the fitting curve are displayed in Figure 7.

Table 4. Magnetic parameters obtained for $Ru_2(OAc)_4Cl$ and for **1** following the model of Equation (2).

	D [cm^{-1}]	$g_{\parallel}$	$g_{\perp}$	g_{av}	R^2
$Ru_2(OAc)_4Cl$	70.6	2.09	2.11	2.10	–
$Ru_2Cu(dpa)_4Cl_2$	52.4	2.01	2.11	2.08	0.99912

The fitted g values are quite similar for $Ru_2(\mu\text{-}O_2CnPr)_4Cl$ and for **1**, which leads to g_{av} = 2.08 (Table 4). The D value calculated for **1** is 52.4 cm^{-1}, which is slightly smaller than the value of 77 cm^{-1} obtained for the Ru dimer in probable relation with weak interactions involving copper.

The EPR spectrum was observed with $g_{\parallel}$ = 1.99 and $g_{\perp}$ = 3.99 (Supporting Information, Figure S6). For an S = 3/2 system with $D >> g\beta H$ one can refer to the effective g values, $g^e = h\nu/\beta H$, such that, for the $Ms = \pm 1/2$ Kramers doublet, $g^e_{\parallel} \approx g_{\parallel}$ and $g^e_{\perp} \approx 2g_{\perp}[1 - (3/16)(g_{\perp}\beta H/D^2)]$. For a large D value as obtained in this complex, $g^e_{\perp} \approx 2g_{\perp}$, which thus leads to a g_{av} value of 2.00 close to the magnetic data. Once again, the small difference should be assigned to the small interactions between the Ru_2 dimer and the Cu ion, which were ignored in the present model.

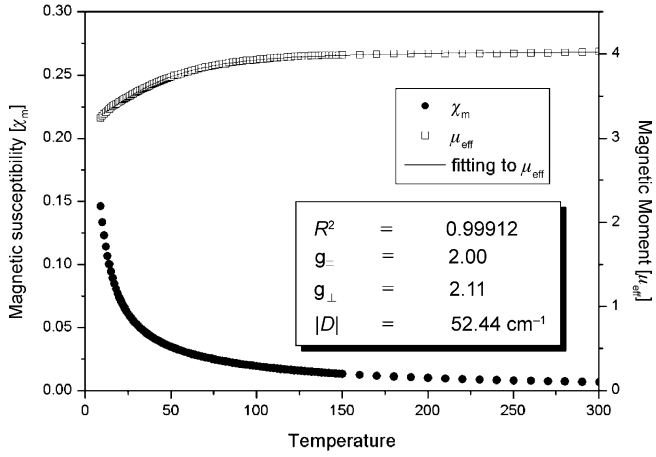

Figure 7. Variable-temperature magnetic susceptibility χ_m (emu mol^{-1}) and magnetic moment μ_{eff} (BM) of **1** at 2000 G and fitting.

The magnetic moment of complex **3** was measured to be 4.27 μ_B at 300 K and gradually decreased below 100 K (Figure 8, top). Spin-only assignments give rise to three

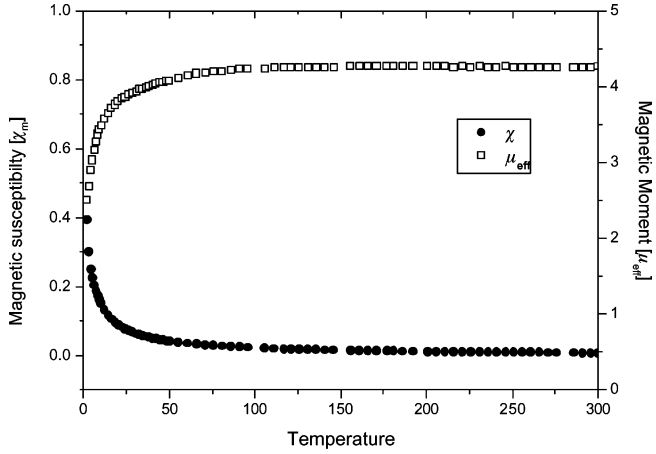

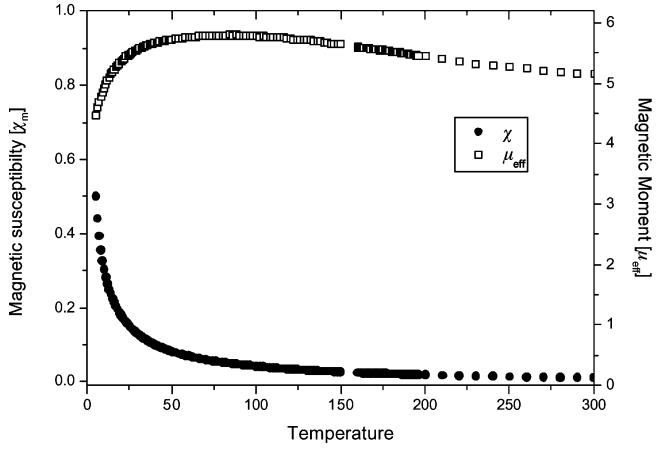

Figure 8. Variable-temperature magnetic susceptibility χ_m (emu mol^{-1}) and magnetic moment μ_{eff} (BM) of **3** and **4** at 2000 G.

possible models: (i) $S = (3/2, 1/2)$ for $[Ru_2]^{5+}$ and Ni^+, which corresponds to $\mu_{eff} = 4.30\ \mu_B$; (ii) $S = (1, 1)$, which leads to $\mu_{eff} = 4.00\ \mu_B$; and (iii) consider that the magnetic centers are strongly interacting, either ferro- or antiferromagnetically, and should not be considered separately. Even though DFT calculations support some through-space connection between the magnetic centers, it appears that this coupling should be weak and antiferromagnetic. A tentative fitting carried out by assuming a negligible D value yielded a J value of $-2.8\ cm^{-1}$. It is clear however that the high correlation between J and D can be neither neglected nor approached from any tentative guess. We think that an appropriate solution to this problem is beyond the scope of the present work.

This magnetic behavior of oxidized complex **2** is strikingly similar to that of **3**, where $\mu_{eff} = 4.30\ \mu_B$ at 300 K, which gradually decreases below 100 K. This suggests a strong similarity between the electronic structures of both complexes: a conjecture confirmed by theoretical modeling. Complexes **2** and **3** are EPR silent. No signal is usually observed for systems with $S = 2$ and large D values. Finally, complex **4** displays a μ_{eff} value of $5.15\ \mu_B$ at 300 K, which then reaches a maximum of $5.80\ \mu_B$ at 88 K (Figure 8, bottom). These values are intermediate between the spin-only assignments considering either separate $[Ru_2]^{5+}$ and $[Ni]^{2+}$ magnetic centers ($S = 3/2, 1$; $\mu_{eff} = 4.79\ \mu_B$) or an ensemble with $S = 5/2$, corresponding to $\mu_{eff} = 5.91\ \mu_B$. The EPR spectrum of complex **4** at 4 K (Supporting Information, Figure S7) shows a strong signal at $g^e_{\perp} = 6.26$ and a weak peak at $g^e_{\parallel} = 2.05$, which is typical of a system with $S = 5/2$ when D is large ($g^e_{\parallel} \approx g_{\parallel}$, $g^e_{\perp} \approx 3g_{\perp}$).[24]

Summary and Conclusion

The dipyridylamide ligand was used to stabilize a new type of heterometallic framework, combining in a linear arrangement a ruthenium dimer characterized by a short Ru–Ru distance and a third metal atom, either Cu or Ni. In spite of a severe disorder affecting the crystal structure, the nonsymmetric nature of the metal framework could be assessed from X-ray diffraction and was confirmed by the presence of eight distinct peaks in the NMR spectra of both $Ru_2M(dpa)_4Cl_2$ complexes. The structure of the Ru dimer in $Ru_2M(dpa)_4Cl_2$ is reminiscent of the mixed-valent diruthenium complexes $Ru_2(\mu\text{-}O_2CR)_4Cl$, and the new complexes indeed display a peak in the near-IR region that appears typical of mixed-valence behavior. DFT calculations confirm that complexes **1** and **3** depart from the neutral complexes of polypyridylamide characterized previously, in which all metal atoms are assigned the same oxidation state II. The $[M–M–M']^{6+}$ framework of the present complexes is better described in terms of a $[Ru_2]^{5+}$ moiety with a $(\sigma)^2(\pi)^4(\delta)^2(\delta^*)^1(\pi^*)^2$ electronic configuration; the third metal atom is formally M^+. Cyclic voltammetry points out the occurrence in both $Ru_2Cu(dpa)_4Cl_2$ and $Ru_2Ni(dpa)_4Cl_2$ of two reversible oxidation events. The monooxidized product could be synthesized and the oxidation was shown from spectroelectrochemical analysis and DFT calculations to occur on the heterometallic center. The second oxidation process was characterized by the appearance of a transition of low energy (≈ 1100 nm), which was tentatively assigned to the removal of an electron from the π* orbital of the $[Ru_2]^{5+}$ moiety to generate a first-order Jahn–Teller distortion. $Ru_2Cu(dpa)_4Cl_2$ displays a magnetic behavior reminiscent of that of $Ru_2(\mu\text{-}O_2C\textit{n}Pr)_4Cl$. For $Ru_2Ni(dpa)_4Cl_2$ as for $[Ru_2Cu(dpa)_4Cl_2]^+$, the observed magnetic moment results from the coupling between the spin of the ruthenium dimer ($S = 3/2$) and that of the heterometallic center ($S = 1/2$). The structure and the characteristics of the complexes suggest that dipyridylamide and other ligands belonging to the same family can open the way to the assembly of linear, heterometallic strings by combining and tuning the magnetic and spectroscopic properties of widely different transition-metal complexes.

Experimental Section

Computational Method: Calculations and full geometry optimizations on complexes **1**, **2**, **3**, and **4** were carried out by assuming C_4 symmetry and by using the density functional theory (DFT) formalism with the spin-unrestricted option, as implemented in the Gaussian03 software,[25] with the B3LYP exchange-correlation functional. All electron valence double-ζ basis sets (D95V) were used to describe C, N, and H atoms. Atoms belonging to the coordination sphere of metals, namely N and Cl, were described by means of full double-ζ basis sets augmented with one d-type polarization function (D95*). Los Alamos core potentials were used to model the neon core of Ni and Cu and the 3s3p3d core of Ru. The valence shell of all types of metal atoms was described at the double-ζ level (LanL2DZ basis).

Materials: Manipulations were performed under an atmosphere of argon by using standard Schlenk techniques. Solvents were purified by standard methods and freshly distilled under an atmosphere of nitrogen prior to use. Bis(2-pyridyl)amine and $Ru_2(OAc)_4Cl$ were synthesized by using published procedures.[26]

Physical Measurements: Absorption spectra were recorded with a Varian Carry 50 spectrophotometer. IR spectra were obtained with a Nicolet Fourier-Transform in the range 500–4000 cm^{-1}. FAB mass spectra were obtained with a JEOL HX-110 HF double-focusing spectrometer operating in the positive ion detection mode. Magnetic susceptibility values were collected with a Quantum external magnetic field of 2000 G. Electrochemistry measurements were carried out with a CH Instruments equipment (Model 750A) with the use of CH_2Cl_2 as the solvent with 0.1 M TBAP and 1 mM analytes. Cyclic voltammetry was recorded with a homemade three-electrode cell equipped with a BAS glossy carbon (0.07 cm^2) disk as the working electrode, a platinum wire as the auxiliary electrode, and a homemade Ag/AgCl (saturated) reference electrode. The reference electrode was separated from the bulk solution by a double junction filled with electrolyte solution. Potentials are reported versus Ag/AgCl (saturated) and referenced to the ferrocene–ferrocenium ($[Cp_2Fe]/[Cp_2Fe]^+$) couple, which occurs at $E_{1/2} = +0.54$ V vs. Ag/AgCl (saturated). The working electrode was polished with 0.03 lm alumina on Buehler felt pads and was subjected to ultrasound for 1 min prior to each experiment. The reproducibility of individual potential values was within ±5 mV. Optical transparent thin layer electrochemical (OTTLE) spectra were obtained by using

a 1-mm UV cell, a 100-mesh platinum gauze as a working electrode, a platinum wire as an auxiliary electrode, and a Ag/AgCl (saturated) reference electrode.

$Ru_2Cu(dpa)_4Cl_2$ (1): In a 100-mL round-bottomed flask, Hdpa (171 mg, 1 mmol), $CuCl_2·2H_2O$ (56 mg, 0.333 mmol), and $Ru_2(OAc)_4Cl$ (118 mg, 0.25 mmol) were dissolved in naphthalene (20 g). The mixture was then heated to ca. 160 °C and kept at this temperature for 20 min. *t*BuOK (122 mg, 1.1 mmol) was then dissolved in *t*BuOH and slowly dropped into this solution. After the base was added, the solution was immediately heated to 220 °C for 30 min. LiCl (200 mg) was added to this solution as a source of chlorine axial ligand. After cooling to ca. 50 °C, hexane (100 mL) was added to this solution and filtered. The crude material was washed with hexane (3×100 mL) to remove naphthalene, and CH_2Cl_2 (100 mL) was added to extract the product. The extract was then condensed to 10 mL. Hexane (20 mL) was added to this solution prior to filtration. Another extraction was then carried with CH_2Cl_2 and the same procedure was repeated two times. The crystal was formed by layering the CH_2Cl_2 solution with ether. Yield: 22 mg, 9%. ^{1}H NMR (400 MHz, CD_2Cl_2, 25 °C): δ (integral, half width) = 35.64 (1 H, J = 52 Hz), 29.03 (1 H, J = 48 Hz), 15.27 (1 H, J = 72 Hz), –0.59 (1 H, J = 296 Hz), –17.70 (1 H, J = 96 Hz), –23.73 (1 H, J = 91 Hz), –31.06 (1 H, J = 48 Hz), –54.16 (1 H, J = 60 Hz) ppm. IR (KBr): $\tilde{\nu}$ = 457.05, 514.90, 539.97, 557.33, 740.53, 748.25, 766.57, 840.81, 873.60, 1022.09, 1056.80, 1111.76, 1158.04, 1238.08, 1286.29, 1311.36, 1350.89, 1424.17, 1462.74, 1593.88, 1602.56 cm^{-1}. MS (FAB): m/z = 1017 $[M + H]^+$. UV/Vis (CH_2Cl_2): λ (ε) = 302 (5.85×10^4), 336 (sh., 3.95×10^4), 470 (6.58×10^3), 568 (2.53×10^3), 902 (4.58×10^3) nm. $C_{40}H_{32}Cl_2CuN_{12}Ru_2$ (1016.96): calcd. C 47.22, H 3.17, N 16.52; found C 47.12, H 3.15, N 16.43.

$Ru_2Ni(dpa)_4Cl_2$ (3): In a 100-mL round-bottomed flask, Hdpa (171 mg, 1 mmol), $NiOAc_24H_2O$ (63 mg, 0.25 mmol), and $Ru_2(OAc)_4Cl$ (118 mg, 0.25 mmol) were dissolved in naphthalene (20 g). The mixture was then heated to ca. 220 °C and kept at this temperature for 2 h. LiCl (200 mg) was added to this solution as a source of chlorine axial ligand. After 30 min, this solution was cooled to ca. 50 °C, and hexane (100 mL) was added to this solution and then filtered. The crude material was washed with hexane (3×100 mL) to remove naphthalene. CH_2Cl_2 (100 mL) was added to extract the product. The extract was then condensed to 10 mL. Hexane (20 mL) was added to this solution prior to filtration. Another extraction was then carried with CH_2Cl_2, and the same procedure was repeated two times. The crystal was formed by layering the CH_2Cl_2 solution with ether. Yield: 122 mg, 49%. ^{1}H NMR (400 MHz, CD_2Cl_2, 25 °C): δ (integral, half width) = 124.48 (1 H, J = 236 Hz), 51.03 (1 H, J = 100 Hz), 39.67 (1 H, J = 96 Hz), 33.30 (1 H, J = 208 Hz), 7.34 (1 H, J = 564 Hz), –7.99 (1 H, J = 316 Hz), –24.07 (1 H, J = 372 Hz), –52.01 (1 H, J = 508 Hz) ppm. IR (KBr): $\tilde{\nu}$ = 457.05, 514.95, 540.07, 557.38, 740.54, 748.27, 766.54, 840.81, 873.61, 1022.11, 1056.82, 1110.78, 1158.04, 1238.08, 1286.29, 1311.36, 1350.89, 1424.19, 1462.76, 1593.79, 1604.54 cm^{-1}. MS (FAB): m/z = 1013 $[M + H]^+$. UV/Vis (CH_2Cl_2): λ (ε) = 292 (6.08×10^4), 342 (3.59×10^4), 454 (7.44×10^3), 478 (5.59×10^3), 898 (5.80×10^3) nm. $C_{40}H_{32}Cl_2N_{12}NiRu_2$ (1011.97): calcd. C 47.45, H 3.19, N 16.60; found C 47.11, H 3.12, N 16.23.

General Procedure for the Preparation of $[Ru_2M(dpa)_4Cl_2]$-$PF_6CH_2Cl_2H_2O$, M = Cu (2); Ni (4): In a flask, $Ru_2M(dpa)_4Cl_2$ (0.1 mmol) and ferrocenium hexafluorophosphate (0.1 mmol) were dissolved in CH_2Cl_2 (20 mL) and MeOH (5 mL) and stirred for 1 h. The mixture was then filtered. This solution was condensed to 5 mL and recrystallized with ether. The crude material was dissolved in CH_2Cl_2 and layered with hexane. After a week, dark brown crystals were formed and collected.

$[Ru_2Cu(dpa)_4Cl_2]PF_6$ (2): Yield: 89 mg, 88%. IR (KBr): $\tilde{\nu}$ = 456.08, 513.94, 539.97, 557.33, 740.53, 748.25, 766.57, 840.81, ((P–F) 846), 874.56, 1014.37, 1022.09, 1056.80, 1110.80, 1157.08, 1238.08, 1284.36, 1311.36, 1350.89, 1423.21, 1462.74, 1548.56, 1592.91, 1602.56 cm^{-1}. MS (FAB): m/z = 1017 $[M + H]^+$. UV/Vis (CH_2Cl_2): λ (ε) = 292 (4.79×10^4), 340 (sh., 3.38×10^4), 458 (6.67×10^3), 482 (5.02×10^3), 870 (5.56×10^3) nm. $C_{40}H_{32}Cl_2CuF_6N_{12}PRu_2$ (1161.93): calcd. C 41.33, H 2.77, N 14.46; found C 41.12, H 2.69, N 14.43.

$[Ru_2Ni(dpa)_4Cl_2]PF_6$ (4): Yield: 83 mg, 82%. IR (KBr): $\tilde{\nu}$ = 457.3, 539.87, 557.13, 740.33, 749.22, 763.52, 840.84, ν(P–F) 845, 874.66, 1017.37, 1022.13, 1056.76, 1110.89, 1156.09, 1238.15, 1284.36, 1311.36, 1350.89, 1423.21, 1462.74, 1548.56, 1593.04, 1602.57 cm^{-1}. MS (FAB): m/z = 1013 $[M + H]^+$. UV/Vis (CH_2Cl_2): λ (ε) = 291 (5.85×10^4), 341 (2.96×10^4), 452 (6.98×10^3), 473 (4.63×10^3), 9.04 (7.46×10^3) nm. $C_{40}H_{32}Cl_2F_6N_{12}NiPRu_2$ (1156.93): calcd. C 41.51, H 2.79, N 14.52; found C 41.19, H 2.72, N 14.41.

Supporting Information (see footnote on the first page of this article): Cartesian coordinates of the DFT/B3LYP optimized structures of **1**, **2**, **3**, and **4**; ORTEP views of **2**, **3**, and **4**. ^{1}H NMR spectra of **1** and **3**; diagram of metal orbitals calculated for the ground states of **2** and **4**; EPR spectra of **1** and **4**.

CCDC-666210, -666211, -666212, and -666213 contain the supplementary crystallographic data for this paper. These data can be obtained free of charge from The Cambridge Crystallographic Data Centre via www.ccdc.cam.ac.uk/data_request/cif.

Acknowledgments

The authors acknowledge the CNRS, the Ministère de l'Education Nationale de l'Enseignement Supérieur et de la Recherche (MENESR, Paris, France), the National Science Council, and the Ministry of Education of Taiwan for financial support. Calculations were shared between the IDRIS (CNRS, Orsay, France), the CINES (Montpellier, France), and the NCHC (Taiwan) computer centers.

[1] a) J. F. Berry in *Multiple Bonds between Metal Atoms*, 3rd ed. (Eds.: F. A. Cotton, C. A. Murillo, R. A. Walton), Springer-Science and Business Media, Inc., New York, **2005**; b) C.-Y. Yeh, C.-C. Wang, C.-h. Chen, S.-M. Peng in *Nano Redox Sites: Nano-Space Control and its Applications* (Ed.: T. Hirao), Springer, Berlin, **2006**, ch 5, pp. 85–117.

[2] a) L.-G. Zhu, S.-M. Peng, *Wuji Huaxue Xuebao* **2002**, *18*, 117; b) J. K. Bera, K. R. Dunbar, *Angew. Chem. Int. Ed.* **2002**, *41*, 4453.

[3] a) S.-Y. Lin, I.-W. P. Chen, C-h. Chen, M.-H. Hsieh, C.-Y. Yeh, T.-W. Lin, Y.-H. Chen, S.-M. Peng, *J. Phys. Chem. B* **2004**, *108*, 959; b) D.-H. Chae, J. F. Berry, S. Jung, F. A. Cotton, C. A. Murillo, Z. Yao, *Nano Lett.* **2006**, *6*, 165; c) I.-W. P. Chen, M.-D. Fu, W.-H. Tseng, J.-Y. Yu, S.-H. Wu, C.-J. Ku, C.-h. Chen, S.-M. Peng, *Angew. Chem. Int. Ed.* **2006**, *45*, 5814; d) I. P.-C. Liu, M. Bénard, H. Hasanov, I.-W. P. Chen, W.-H. Tseng, M.-D. Fu, M.-M. Rohmer, C-h. Chen, G.-H. Lee, S.-M. Peng, *Chem. Eur. J.* **2007**, *13*, 8667.

[4] M.-M. Rohmer, I. P.-C. Liu, J.-C. Lin, M.-J. Chiu, C.-H. Lee, G.-H. Lee, M. Bénard, X. López, S.-M. Peng, *Angew. Chem. Int. Ed.* **2007**, *46*, 3533.

[5] I. P-C. Liu, G.-H. Lee, S.-M. Peng, M.-M. Rohmer, M. Bénard, *Inorg. Chem.* **2007**, *46*, 9602.

[6] M. Nippe, J. F. Berry, *J. Am. Chem. Soc.* **2007**, *129*, 12684.

[7] a) C.-H. Chien, J.-C. Chang, C.-Y. Yeh, G.-H. Lee, J.-M. Fang, Y. Song, S.-M. Peng, *Dalton Trans.* **2006**, 2106; b) C.-H. Chien, J.-C. Chang, C.-Y. Yeh, G.-H. Lee, J.-M. Fang, Y. Song, S.-M. Peng, *Dalton Trans.* **2006**, 3249; c) H. Hasanov, U.-K. Tan, G.-H. Lee, S.-M. Peng, *Inorg. Chem. Commun.* **2007**, *10*, 983.

[8] A. K. Chakravarty, F. A. Cotton, D. A. Tocher, *Inorg. Chem.* **1985**, *24*, 172.

[9] a) J.-T. Sheu, C.-C. Lin, I. Chao, C.-C. Wang, S.-M. Peng, *Chem. Commun.* **1996**, 315; b) C.-K. Kou, I. P.-C. Liu, C.-Y. Yeh, C.-H. Chou, T.-B. Tsao, G.-H. Lee, S.-M. Peng, *Chem. Eur. J.* **2007**, *13*, 1442.

[10] J. F. Berry, F. A. Cotton, P. Lei, C. A. Murillo, *Inorg. Chem.* **2003**, *42*, 377.

[11] M. Bénard, J. F. Berry, F. A. Cotton, C. Gaudin, X. López, C. A. Murillo, M.-M. Rohmer, *Inorg. Chem.* **2006**, *45*, 3932.

[12] a) R. Clérac, F. A. Cotton, L. M. Daniels, K. R. Dunbar, K. Kirschbaum, C. A. Murillo, A. A. Pinkerton, A. J. Schultz, X. Wang, *J. Am. Chem. Soc.* **2000**, *122*, 6226 and references cited therein; b) M.-M. Rohmer, A. Strich, M. Bénard, J.-P. Malrieu, *J. Am. Chem. Soc.* **2001**, *123*, 9126; c) D. A. Pantazis, J. E. McGrady, *J. Am. Chem. Soc.* **2006**, *128*, 4128.

[13] a) J. F. Berry, F. A. Cotton, T. Lu, C. A. Murillo, X. Wang, *Inorg. Chem.* **2003**, *42*, 3595; b) P. Kiehl, M.-M. Rohmer, M. Bénard, *Inorg. Chem.* **2004**, *43*, 3151.

[14] R. Clérac, F. A. Cotton, L. M. Daniels, K. R. Dunbar, C. A. Murillo, X. Wang, *J. Chem. Soc., Dalton Trans.* **2001**, 386.

[15] X. López, M. Bénard, M.-M. Rohmer, *J. Mol. Struct.: THEOCHEM* **2006**, *777*, 53.

[16] N. Benbellat, M.-M. Rohmer, M. Bénard, *Chem. Commun.* **2001**, 2368.

[17] a) I. Mayer, *Chem. Phys. Lett.* **1983**, *97*, 270; b) I. Mayer, *Int. J. Quantum Chem.* **1986**, *29*, 477.

[18] V. M. Miskowski, H. B. Gray, *Inorg. Chem.* **1988**, *27*, 2501 and references cited therein.

[19] J. G. Norman Jr, G. E. Renzoni, D. A. Case, *J. Am. Chem. Soc.* **1979**, *101*, 5256.

[20] M. H. Chisholm, G. Christou, K. Folting, J. C. Huffman, C. A. James, J. A. Samuels, J. L. Wesemann, W. A. Woodruff, *Inorg. Chem.* **1996**, *35*, 3643 and references cited therein.

[21] a) F. A. Cotton, B. A. Frenz, E. Pedersen, T. R. Webb, *Inorg. Chem.* **1975**, *14*, 391; b) T. Malinski, D. Chang, F. N. Feldmann, J. L. Bear, K. M. Kadish, *Inorg. Chem.* **1983**, *22*, 3225; c) K. Chakravarty, F. A. Cotton, D. A. Tocher, *J. Am. Chem. Soc.* **1984**, *106*, 6409.

[22] a) J. Telser, R. S. Drago, *Inorg. Chem.* **1984**, *23*, 3114; b) J. Telser, R. S. Drago, *Inorg. Chem.* **1985**, *24*, 4765.

[23] a) C. J. O'Connor, *Prog. Inorg. Chem.* **1982**, *29*, 203; b) M. A. S. Aquino, *Coord. Chem. Rev.* **1998**, *170*, 141.

[24] G. C. Brackett, P. L. Richards, W. S. Caughey, *J. Chem. Phys.* **1971**, *54*, 4383.

[25] M. J. Frisch, G. W. Trucks, H. B. Schlegel, G. E. Scuseria, M. A. Robb, J. R. Cheeseman, J. A. Montgomery, Jr., T. Vreven, K. N. Kudin, J. C. Burant, J. M. Millam, S. S. Iyengar, J. Tomasi, V. Barone, B. Mennucci, M. Cossi, G. Scalmani, N. Rega, G. A. Petersson, H. Nakatsuji, M. Hada, M. Ehara, K. Toyota, R. Fukuda, J. Hasegawa, M. Ishida, T. Nakajima, Y. Honda, O. Kitao, H. Nakai, M. Klene, X. Li, J. E. Knox, H. P. Hratchian, J. B. Cross, C. Adamo, J. Jaramillo, R. Gomperts, R. E. Stratmann, O. Yazyev, A. J. Austin, R. Cammi, C. Pomelli, J. W. Ochterski, P. Y. Ayala, K. Morokuma, G. A. Voth, P. Salvador, J. J. Dannenberg, V. G. Zakrzewski, S. Dapprich, A. D. Daniels, M. C. Strain, O. Farkas, D. K. Malick, A. D. Rabuck, K. Raghavachari, J. B. Foresman, J. V. Ortiz, Q. Cui, A. G. Baboul, S. Clifford, J. Cioslowski, B. B. Stefanov, G. Liu, A. Liashenko, P. Piskorz, I. Komaromi, R. L. Martin, D. J. Fox, T. Keith, M. A. Al-Laham, C. Y. Peng, A. Nanayakkara, M. Challacombe, P. M. W. Gill, B. Johnson, W. Chen, M. W. Wong, C. Gonzalez, J. A. Pople, *Gaussian 03*, Revision B.05, Gaussian, Inc., Pittsburgh PA, **2003**.

[26] a) K. S. Huang, M. J. Kurth, *J. Org. Chem.* **2002**, *67*, 2382; b) T. A. Stephenson, G. J. Wilkinson, *Inorg. Nucl. Chem.* **1966**, *28*, 2285.

Received: October 26, 2007
Published Online: March 3, 2008

